Exp Fluids (2009) 46:799–810
DOI 10.1007/s00348-009-0654-1

RESEARCH ARTICLE

Design and development considerations for biologically inspired flapping-wing micro air vehicles

Kevin D. Jones · Max F. Platzer

Received: 4 June 2008 / Revised: 25 March 2009 / Accepted: 27 March 2009 / Published online: 19 April 2009

Abstract In this paper, the decade of numerical and experimental investigations leading to the development of the authors' unique flapping-wing micro air vehicle is summarized. Early investigations included the study of boundary layer energization by means of a small flapping foil embedded in a flat-plate boundary layer, the reduction of the recirculatory flow region behind a backward-facing step by means of a small flapping foil, and the reduction or suppression of flow separation behind blunt or cusped airfoil trailing edges by flapping a small foil located in the wake flow region. These studies were followed by systematic investigations of the aerodynamic characteristics of single flapping airfoils and airfoil combinations. These unsteady flows were described using flow visualization, laser-Doppler velocimetry in addition to panel and Navier–Stokes computations. It is then shown how this flapping-wing database was used to conceive, design and develop a micro air vehicle which has a fixed wing for lift and two flapping wings for thrust generation. While animal flight is characterized by a coupled force generation, the present design appears to separate lift and thrust. However, in fact, the performance of one surface is closely coupled to the other surfaces.

1 Introduction

The micro air vehicle (MAV) configuration shown in Fig. 1 was first flown in December 2002. Since that time variations of it have been flown many times. The third generation model shown on the right has a span of 25 cm, a length of 17 cm, a flying weight of about 13 g, and flies for about 15 min on a rechargeable lithium-polymer battery at flight speeds between 2 and 5 m/s. The MAV has a fixed wing and two flapping wings mounted downstream but very near the trailing edge of the fixed wing. The flapping wings oscillate in counterphase so that while one wing, for example, moves up the other moves down and vice versa. Therefore the joint center of gravity is essentially unaffected by the oscillations of the two wings. Furthermore, and contrary to animal flight, the amplitude of the oscillations is constant along the span.

Clearly, there is no counterpart to this vehicle in nature. Yet, one important element found in nature was adopted in its design and development, namely wing flapping. As is well known, early pioneers of aeronautical engineering, such as Lilienthal (1992) were convinced that the key to flight with heavier-than-air vehicles was to be found in emulating bird flight as closely as possible. Earlier attempts to do so are documented by Dalton (1999). Lilienthal contributed greatly to the understanding of flapping-wing aerodynamics. In particular, he correctly identified the drag reduction (or thrust generation) caused by wing flapping. However, the success of the Wright brothers in 1903 with the fixed-wing aircraft concept soon convinced the aeronautical engineering community to regard the flapping-wing aircraft concept as unpromising for further development and, indeed, throughout the whole twentieth century few attempts were made to build flapping-wing vehicles. It was only toward the end of the century that a new type of air vehicle of greatly diminished size, the micro air vehicle, triggered a re-examination of the flapping-wing aircraft concept, primarily due to the necessarily small Reynolds numbers they would experience, typically from a few thousand to a few tens of thousands.

K. D. Jones (✉) · M. F. Platzer
Naval Postgraduate School, Monterey, CA, USA
e-mail: jones@nps.edu

M. F. Platzer
e-mail: mplatzer@nps.edu

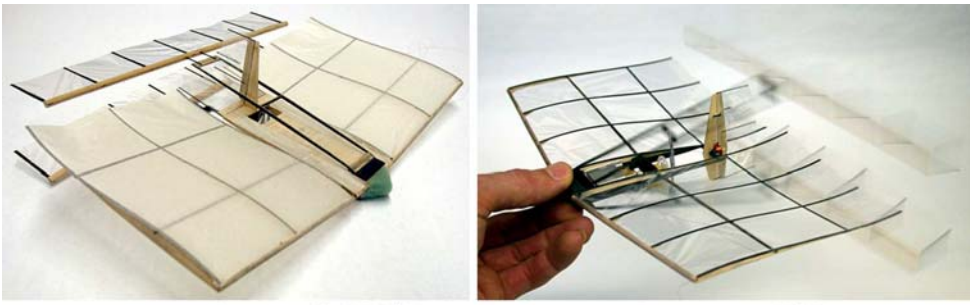

Fig. 1 The authors' unconventional fixed/flapping-wing MAV design. The large fore-wing provides most of the lift while the biplane-pair of trailing wings provide the thrust, but the interaction between them provides the necessary efficiency for flight. The first generation model had throttle control, and first flew in 2002. The third generation had two-channel control, a modular construction, 25 cm span, 17 cm length and 13 g weight, and flew for 15 min at 2–5 m/s on a rechargeable battery

In this paper, we would like to document the basic design philosophy which led us to the configuration shown in Fig. 1. This philosophy can be summarized by stating that we wanted to make maximum use of the existing knowledge about flapping wing aerodynamics. To this end, it was obvious that we should concentrate on high-aspect-ratio wings because much more was (and still is) known about two-dimensional flapping airfoil aerodynamics than about highly three-dimensional wing aerodynamics. Therefore, we first summarize the state-of-the-art in the early 1990s at the start of our MAV development effort and then proceed to the description of our experimental and computational investigations. However, in keeping with the emphasis of this journal on experiments we highlight the experimental aspects and mention the computational aspects only to the extent needed for a fuller understanding of our total approach. For additional computational details we refer to the cited references.

2 Knoller–Betz–Katzmayr effect

Although Lilienthal had already achieved a considerable understanding of the basic physics underlying flapping wings, a more definitive theory was first given independently by Knoller (1909) and Betz (1912). Their explanation is shown in Fig. 2 where an airfoil is depicted which executes harmonic plunge oscillations. As the airfoil moves through its mean position (either up or down) the airfoil "sees" an effective angle of attack, α_{eff}, due to the vectorial superposition of its flight speed, V_∞, and the plunge velocity, $z'(t)$. Neglecting viscous and three-dimensional effects a resultant aerodynamic force, N, is generated which is inclined forward. Hence a harmonically varying force component in the flight direction, T, (i.e. thrust) starts to be generated. Katzmayr (1922) verified this effect by exposing an airfoil to an oscillating wind tunnel flow. This work, in turn, stimulated a more detailed analysis by Birnbaum (1924) who applied Prandtl's unsteady thin airfoil theory to this problem. He was the first to give a quantitative prediction of thrust generation due to slowly oscillating airfoils and he was able to show that the oscillating airfoil sheds vortices from its trailing edge (an effect not yet included by Knoller and Betz). Garrick (1936) presented results valid for the complete frequency range based on Theodorsen's (1935) thin airfoil theory. At about the same time von Kármán and Burgers (1934) pointed out that the vortex shedding from a thrust-producing oscillating airfoil occurs in the form of a "reverse" Kármán vortex street.

The generation of this vortex street can be understood by recalling the basic principle of lift generation on an airfoil. To this end it is important to remember that a so-called "starting vortex" is shed from the airfoil trailing edge whenever the airfoil incidence angle is abruptly changed. A sudden increase in angle of attack produces the shedding of a counterclockwise starting vortex. A decrease produces a clockwise vortex. The trailing edge has to be reasonably sharp for this shedding to occur with sufficient strength. A rounded trailing edge greatly diminishes the shedding. Consider now the airfoil as it plunges from above through the mean position. The airfoil "sees" a maximum positive angle of attack at this moment which starts to diminish greatly as it slows down. Hence the angle of attack changes from positive to negative as it reverses and reaches the maximum negative angle of attack as it approaches the mean position from below. Therefore, during this part of the oscillation the airfoil sheds clockwise vorticity which accumulates quickly into the clockwise vortex of the lower row of the reverse Kármán vortex street. Similarly, while the airfoil moves above the mean position it sheds a counterclockwise vortex.

In the early 1990s we were able to predict this vortex shedding behavior with the panel code solutions for

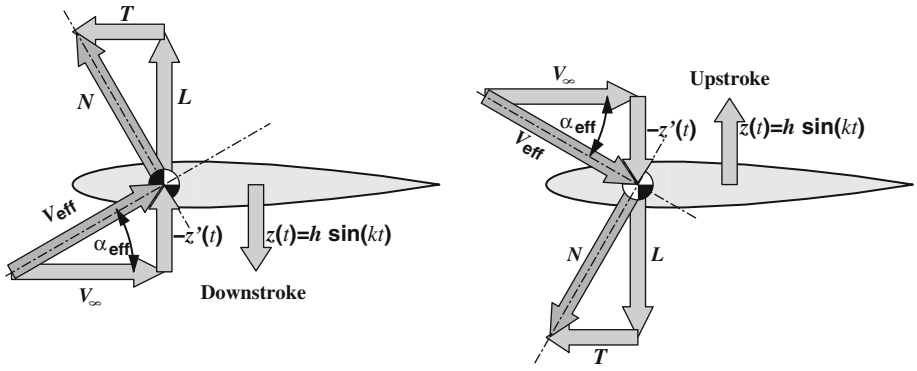

Fig. 2 Schematic illustrating thrust production by a plunging airfoil as posed by Knoller and Betz in 1909 and 1912, respectively

incompressible inviscid flow past oscillating airfoils which we had developed in preceding years for the purpose of studying low-speed airfoil flutter phenomena (Teng 1987; Platzer et al. 1993). These solutions represented a considerable advance over the linearized small amplitude solutions obtained by Birnbaum (1924) and Garrick (1936). However, they left unanswered the effect of viscosity on the thrust and propulsive efficiency predictions of the thin-airfoil and the panel codes. Therefore, we decided to perform visualizations and measurements of the flow over harmonically plunging airfoils.

3 Flow over harmonically plunging airfoils

In Fig. 3 we show a visualization of the reverse Kármán vortex street; called "reverse" because it consists of counterclockwise rotating upper row vortices and clockwise rotating vortices in the lower row. This arrangement is the exact opposite of the classical Kármán vortex street shed, for example, from a stationary cylinder in a low-speed flow where the upper row vortices are turning clockwise and lower row vortices are turning counterclockwise. These visualizations were performed in an Eidetics Model 1520 closed circuit water tunnel. The wing had a 10 mm chord with an airfoil section that approximated a NACA 0012, and was oscillated vertically with a programmable shaker. Dye was injected just upstream of the airfoil above and below the centerline. Flow speed was measured with a TSI LDV system.

The change in vortex shedding from the trailing edge of a stationary airfoil to that from a harmonically plunging airfoil as the amplitude of oscillation is increased for a given frequency of oscillation is shown in Fig. 4. The classical Kármán vortex street shed from the stationary airfoil is shown in (a). As the airfoil starts to oscillate in plunge at a relatively low reduced frequency, $k = 2\pi fc/V_\infty$, and amplitude, h (non-dimensionalized by c), the Kármán vortex street changes into the mushroom-like vortex pattern shown in (b). As the product hk (the peak non-dimensional plunge velocity) is increased, this vortex pattern changes into the pattern shown in (c). A further increase finally produces the reverse Kármán vortex street shown in (d). A comparison of the panel-code computed vortex street with the observed street of (d) shows excellent agreement. However, the panel code could not reproduce the vortex patterns shown in (a), (b) and (c). Hence these flow visualization experiments indicate the inadequacy of inviscid flow computations for low values of frequency and amplitude. On the other hand, they also show that there is a range of flow speed, frequencies and amplitudes where inviscid computations produce good agreement. In particular, when the thrust produced by flapping exceeds the viscous drag coefficient by some margin, and actually to some degree quite far into the dynamic-stall regime.

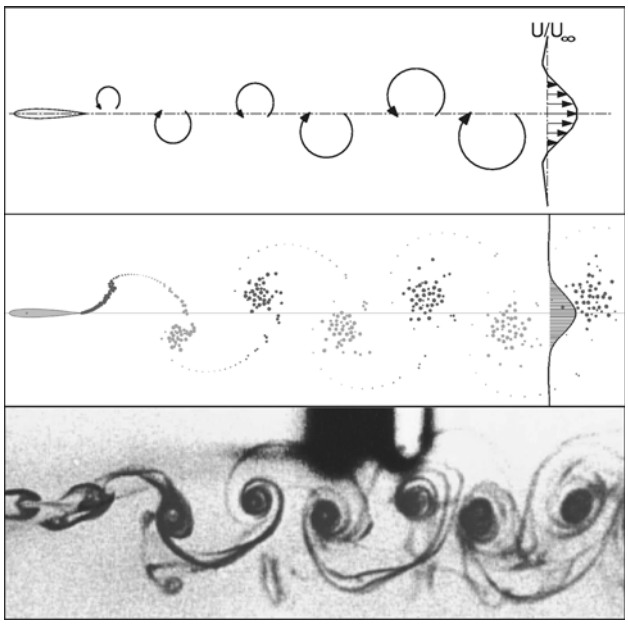

Fig. 3 Vortex arrangement in a thrust-indicative reverse Kármán vortex street: *top* schematic, *middle* panel code, *bottom* experimental. Reduced frequency, k, is 3, non-dimensional plunge amplitude, h, is 0.20, resulting in $hk = 0.60$. For the experiment, $V_\infty = 0.105$ m/s, $f = 5$ Hz, and $Re = 1{,}037$

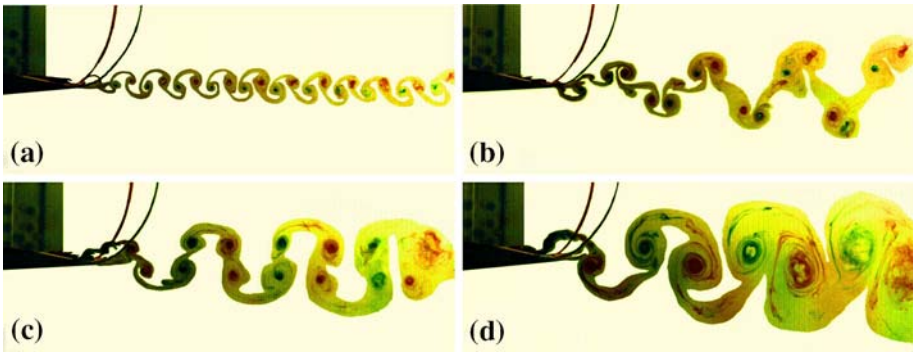

Fig. 4 Transition from normal to reverse Kármán vortex street with increasing *hk* (Lai and Platzer 1999). **a** $hk = 0.0$, **b** $hk = 0.1$, **c** $hk = 0.2$, **d** $hk = 0.4$

These flow visualizations revealed the important fact that previous conclusions drawn from inviscid flow computations can be quite wrong. For example, Garrick's inviscid linearized flow analysis showed that the propulsive efficiency of a harmonically plunging airfoil decreases from values close to 100% at very small reduced frequencies to only 50% for high frequencies. Since the amplitude of oscillation is necessarily limited to small values in linearized theory this type of analysis leads to the conclusion that propulsive efficiency of a harmonically plunging airfoil decreases from values close to 100% at very small reduced frequencies to only 50% for high frequencies. Since the amplitude of oscillation is necessarily limited to small values in linearized theory this type of analysis leads to the conclusion that good efficiencies require flapping at small frequencies. In contrast, (b) and (c) demonstrate that the transition from drag production in (a) to thrust production in (d) occurs by means of increasing the amplitude (at a given frequency). These figures also show that the transition occurs gradually by means of the changes in vortex shedding from (a) through (b) and (c) to (d). The important parameter characterizing the type of vortex shedding therefore has to contain both the frequency and amplitude, usually expressed in terms of the Strouhal number, $St = fA/U_\infty$, where f is the frequency (in Hertz), A the peak-to-peak excursion of the airfoil trailing edge ($2hc$ for a plunging wing) and U_∞ the flow or flight speed. Note that $St = hk/\pi$, and thus the product hk, the maximum non-dimensional plunge velocity, has essentially the same meaning as the Strouhal number.

As is well known, the Kármán vortex shedding from the stationary airfoil in (a) is indicative of airfoil drag. This drag is being reduced as the shedding transitions to the shedding shown in (b) and (c) until net thrust is being generated on the airfoil after transition into the reverse Kármán shedding of (d). This can be understood by realizing that the counterclockwise rotating vortices of the upper row and the clockwise rotating vortices of the lower row entrain flow from the outside so that a higher velocity flow is generated between the two vortex rows. Hence one would expect a jet-like flow to be created if one measures the time-averaged flow, as indicated in Fig. 3. This is

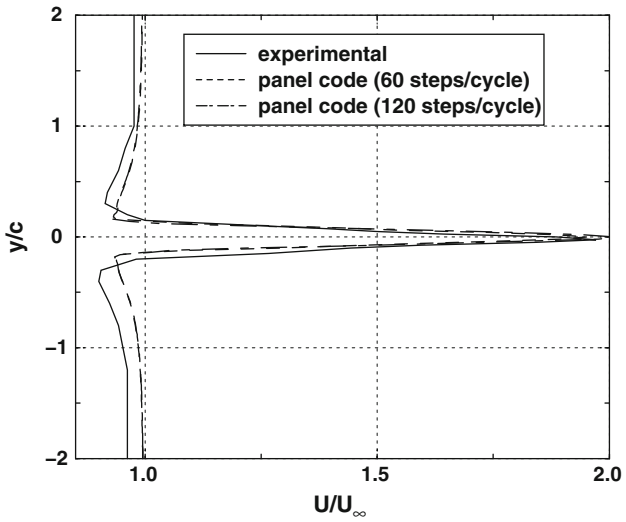

Fig. 5 Measured (LDV) and computed (panel code) time-averaged velocity profile behind the flapping wing for the case shown in Fig. 3

indeed the case. In Fig. 5 we show one of our time-averaged flow measurements (using LDV) in a plane near (but downstream) of the airfoil trailing edge (Jones et al. 1998, 2001; Lai and Platzer 1999). It is seen that the oscillating airfoil indeed generates a distinct jet. It is also seen that the panel-code computed jet profile is in good agreement with the measurement (Fig. 5), again proving that inviscid flow calculations can be quite adequate for certain parameter combinations. The oscillating airfoil therefore imparts momentum to the fluid in the streamwise direction which, in turn, generates a reaction force (thrust) in the opposite direction on the airfoil. The flapping wings of some birds and insects therefore can be considered as a "jet engine" which came into use several times many millions of years before the aircraft jet engine was invented and applied.

A more systematic variation of the amplitude and frequency of plunge oscillation, however, revealed an additional flow regime as soon as the Strouhal number exceeded a certain critical value. As shown in Fig. 6, the shedding then occurs with a finite deflection angle, accompanied by the shedding of additional secondary vorticity. Bratt (1950) shows a similar picture in his report, but makes

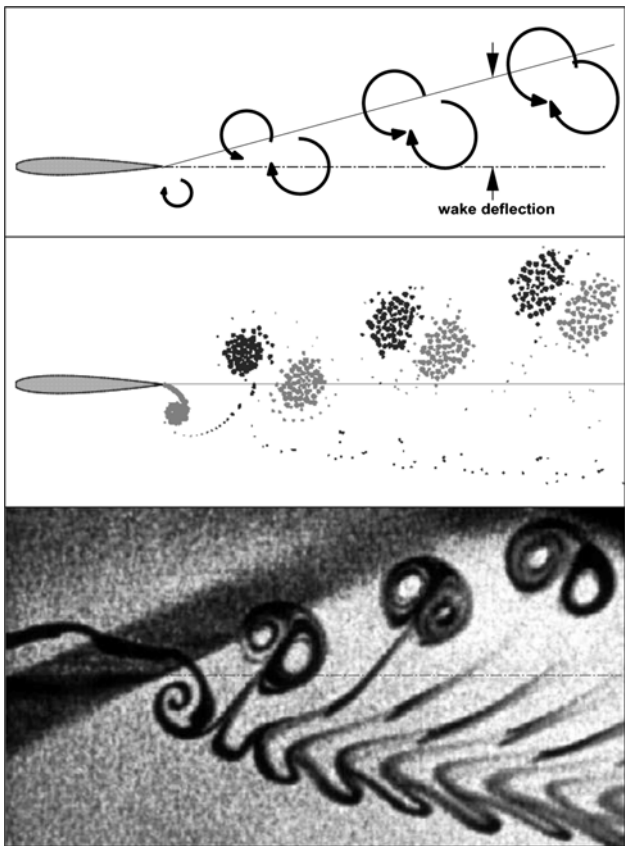

Fig. 6 Vortex arrangement for the deflected-wake vortex street: *top* schematic, *middle* panel code, *bottom* experimental. In this experiment, $k = 12.3$, $h = 0.12$, resulting in $hk = 1.48$. In the experiment, $U_\infty = 0.026$ m/s, $f = 5$ Hz, and $Re = 252$

no comments about this phenomenon. The physical reason for this type of shedding seems to be the shed vortices forming too closely spaced as the frequency is increased. As is also shown in Fig. 6, this deflected jet phenomenon (which generates both thrust and lift on the airfoil) can be predicted with the inviscid panel code. The direction of the jet deflection seemed to depend on the initial starting position of the airfoil. However, Heathcote and Gursul (2004) found in a more recent investigation that the jet switches with a period two orders of magnitude greater than the period of the plunge motion, thus triggering interesting fluid stability questions worthy of future analysis and experimentation. In the water tunnel experiments, the asymmetric wake pattern typically occurred for $hk > 1.0$, although this value is probably dependent on the Reynolds number.

4 Boundary layer and flow separation control by means of harmonically plunging airfoils

As is clear from the preceding discussion, the oscillating airfoil can be regarded as a propeller that entrains a certain

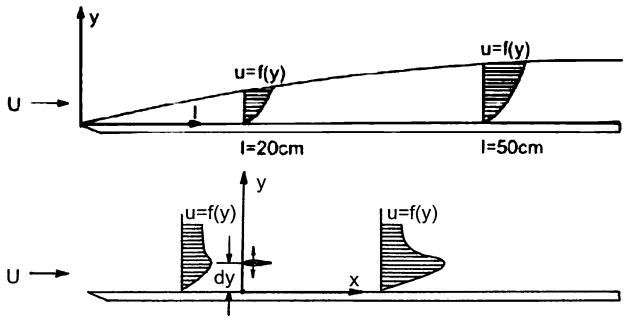

Fig. 7 In the *upper image* a typical boundary layer on a flat plate is shown. In the *lower image* a small airfoil is placed in the boundary layer and flapped. The flapping creates thrust resulting in a jet profile (Dohring 1998)

amount of flow along its span and gives it a certain amount of additional flow momentum. This fact suggested that oscillating airfoils must have potential uses for flow control purposes. Therefore, we thought it might be of interest to study the effect of a small oscillating airfoil mounted in the laminar boundary layer of a flat plate. The arrangement is shown in Fig. 7.

A NACA0012 airfoil of 20 mm chord was mounted in a laminar flat-plate boundary layer. Flow visualization and measurements were performed for different amplitudes and frequencies of the plunging foil. Also, the effect of the distance from the plate was investigated. The experiment was performed in an Eidetics water tunnel. The measurements consisted of LDV flow surveys upstream and downstream of the oscillating airfoil. A typical time-averaged flow profile at a station 0.75 chord lengths downstream of the trailing edge is shown in Fig. 8.

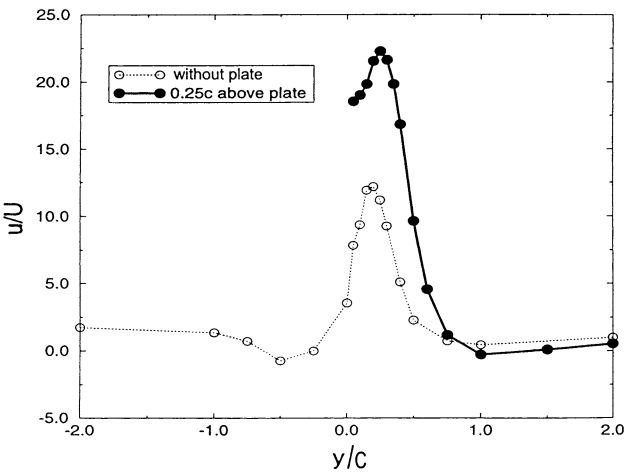

Fig. 8 Measured (LDV) time-averaged velocity profiles in free flow and in the boundary layer of a flat-plate. In the experiment, $h = 0.088c$, $k = 114$, and the Reynolds number was 220. While not shown, velocity measurements very close to the surface of the flat plate show the velocity dropping to zero quite abruptly (Dohring 1998)

It is seen that, compared to the airfoil oscillating in the outside free-stream, the airfoil oscillating in the boundary layer generates a significantly increased jet flow. The flow visualization revealed that the vortex shedding was of the deflected jet type (as discussed in the previous section). The main conclusion from this experiment was that airfoil oscillation close to a flat surface is favorable. Navier–Stokes computations were in substantial agreement with the experimental findings. Details of the Navier–Stokes solver and the results are documented in Dohring (1998).

In Fig. 9 the flow over a stationary airfoil of 28 cm chord length and a maximum thickness of 4.5 cm is shown with either a rounded or cusped trailing edge. The airfoil is at zero angle of attack. A 2 cm chord length airfoil, mounted at a small downstream distance from the trailing edge, is oscillated in plunge with varying amplitude and frequency. This experiment was again carried out in the Eidetics water tunnel. Flow visualization revealed that, depending on the chosen amplitude and frequency of oscillation, the entrainment effect of the oscillating airfoil was strong enough to suppress the flow separation. Systematic variation of the water flow speed and frequency and amplitude of plunge oscillation led to the critical boundary shown in Fig. 10 where the amplitude, h, is plotted on the ordinate and the reduced frequency, k, is plotted along the abscissa. Any combination of parameters to the right of this critical boundary produces complete flow reattachment. Again, complete details are given by Dohring (1998). Results for a range of flapping foil sizes and downstream locations were obtained, with intuitive trends, i.e., smaller flapping wings or further downstream locations required higher hk for reattachment.

In Fig. 11 the flow over a backward-facing step is shown. A harmonically plunging NACA0012 foil of 10 mm chord is mounted in the recirculating flow region caused by a step height of 30 mm. This experiment was also carried out in the Eidetics water tunnel facility of the Naval Postgraduate School. Flow visualization and single-component laser Doppler velocimetry was again used to study the effect of frequency and amplitude of plunge

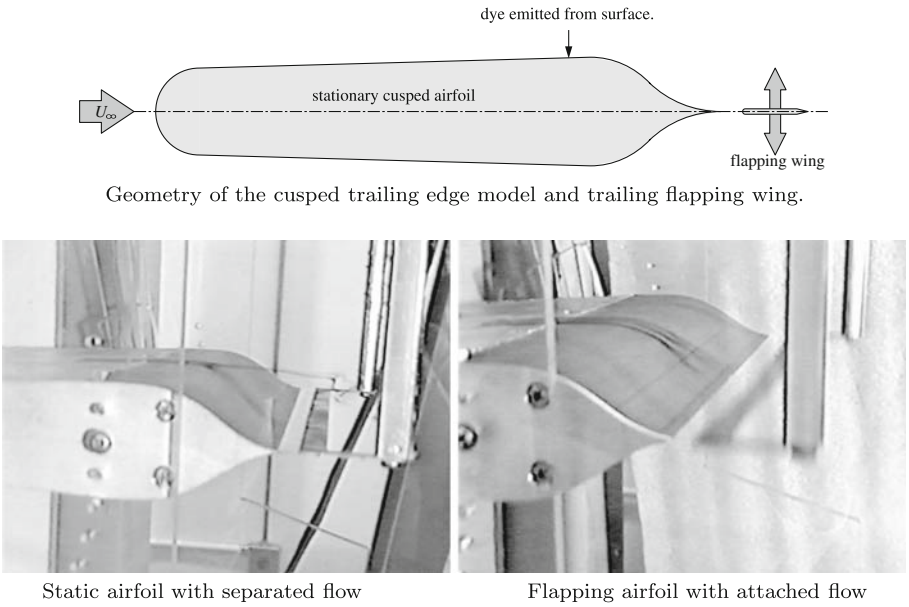

Fig. 9 In the *left image* the trailing airfoil is at rest and the injected dye illustrates massive separation. In the *right image* the trailing wing is flapped, with the entrained flow re-attaching the flow. Results for the main airfoil with rounded trailing edge are similar (Dohring 1998)

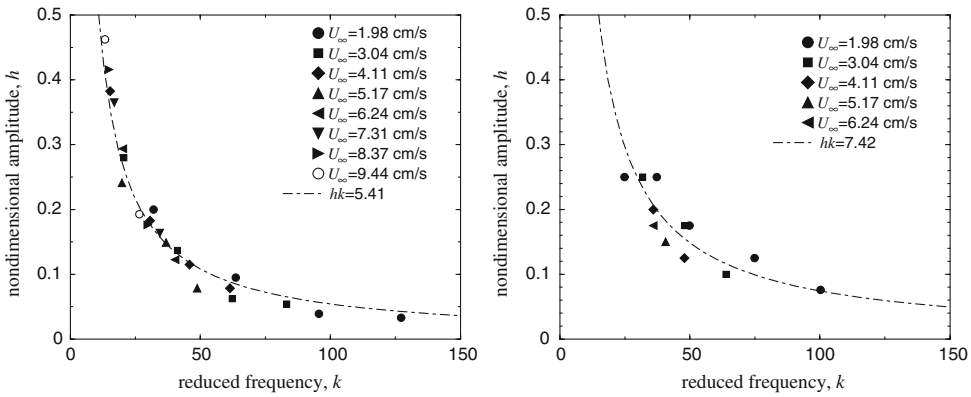

Fig. 10 Critical value of hk for flow reattachment (Dohring 1998). In the *left figure*, a 2 cm chord airfoil placed 0.2c downstream of the cusped trailing edge airfoil is flapped, and the *plotted symbols* indicate the combination of h and k that resulted in reattachment. In the *right figure* similar results are shown for the main airfoil with the round trailing edge, but with the flapping wing 0.25c downstream

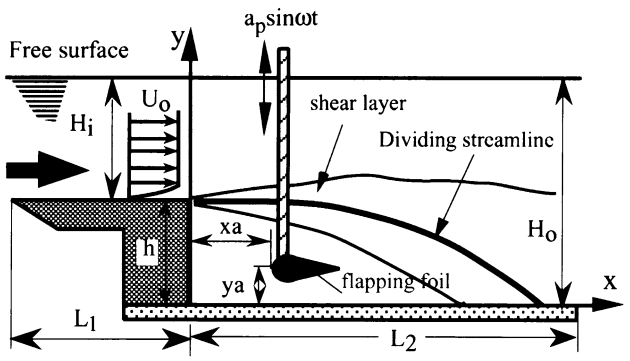

Fig. 11 Schematic of the backward-facing step experiment (Lai et al. 2002). The defining parameters are: $c = 10$ mm, $h = 3c$, $L_1 = 91c$, $L_2 = 70c$, $H_0 = 27c$, $H_i = 24c$, $V_\infty = 0.32$ m/s and *Re* based on step height was 12,700. The step width was $38c$, and the flapping wing was centered $6c$ downstream of the step

oscillation and location of the oscillating foil on the size of the recirculating flow region. This experiment revealed that the strong mixing and entrainment caused by the foil oscillation can reduce the reattachment length by as much as 70%. The measured time-averaged streamlines for the stationary foil and the foil oscillating at 20 Hz with a non-dimensional amplitude of 0.123 are shown in Fig. 12. More details are given by Lai et al. (2002).

The above three experiments led us to the insight that it might be quite beneficial to place an oscillating airfoil close to, but downstream of a stationary airfoil in order to exploit the fact that an aircraft's propulsive efficiency is improved when the air from the wake of the aircraft is used as part of the propulsive stream. Betz (1966) explains this in his book and points out that with wake ingestion the power expended can actually be less than the product of the forward speed and craft drag. At the Douglas Aircraft Company, Smith and Roberts (1947) also proposed to use the boundary layer air for propulsion and Smith (1947) of the General Electric Company quantified the potential benefits of wake ingestion.

Furthermore, the flat-plate boundary layer experiment and inviscid panel code computations for two airfoils, oscillating in counterphase in a biplane arrangement, provided the additional insight that the most promising arrangement might be the closely coupled fixed-wing/oscillating-biplane configuration. The oscillating airfoil flying near a flat surface (or the equivalent biplane airfoils oscillating in counterphase) generate a favorable ground effect (increased thrust and propulsive efficiency). Locating the oscillating biplane airfoils downstream of the fixed wing adds the favorable wake ingestion effect. These two aerodynamic benefits are greatly enhanced by the fact that oscillation in counterphase produces a dynamically balanced configuration, hence eliminates the problem of pitch oscillations induced by the use of single wings.

5 Thrust measurements of oscillating airfoils in biplane arrangement

Having recognized the advantages of the biplane arrangement it remained to select the most suitable oscillation

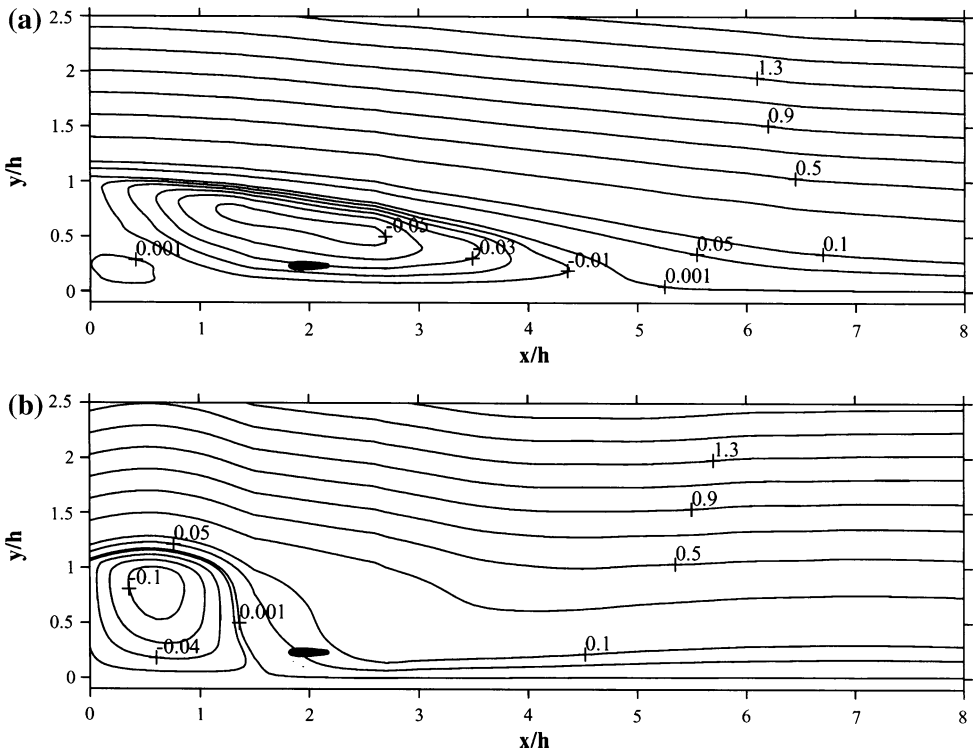

Fig. 12 Mean non-dimensional streamlines with and without flapping illustrating the reduction in the recirculation region (Lai et al. 2002). **a** Stationary foil, **b** Foil flapping at 20 Hz with amplitude $0.123c$

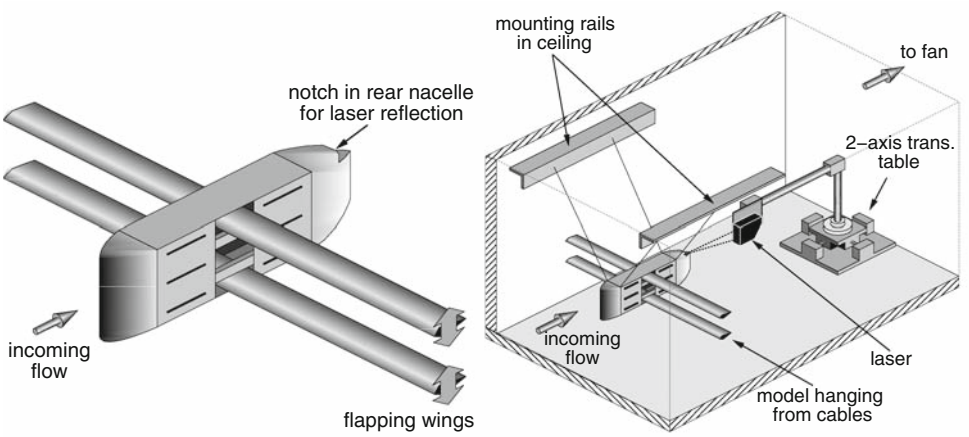

Fig. 13 Large biplane wind-tunnel test model, with 65 mm chord, 1.2 m span wings and a NACA 0014 airfoil section. The model is hung from the ceiling of the test section, and a laser range finder is used to measure its streamwise displacement to calculate thrust or drag

mode. Panel code calculations indicated that the highest propulsive efficiencies are obtained with combined pitch and plunge oscillations if the phase angle between the two modes is approximately 90°. However, experimental confirmation was needed to verify this prediction. Therefore, the model shown in Fig. 13, was built and tested. The two biplane wings could be oscillated in either pitch or plunge. The thrust could be measured quite easily by hanging the model from the wind tunnel ceiling, as shown, and by measuring the small forward movement of the model with a laser range finder as soon as the wing oscillation was turned on. Typical results are shown in Fig. 14 (Jones et al. 2001).

These thrust measurements were quite encouraging and provided the motivation to build a much smaller model (of potential MAV size) and to repeat the thrust measurements. This model is shown in Fig. 15, with a similar pendulum

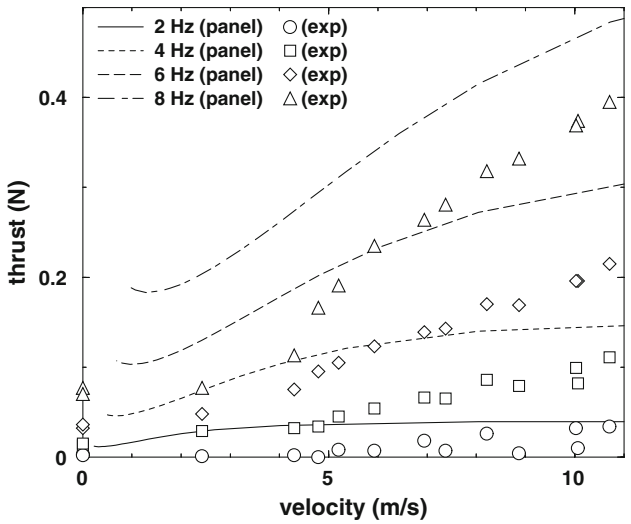

Fig. 14 Predicted and measured thrust for the large biplane model. Reynolds numbers ranged from 0 to 50,000, and the motion of each wing was pure plunge with amplitude 0.4*c*. Mean separation between the wings was 1.4*c*

experimental setup (shown in Fig. 16) to measure the very small drag/thrust quantities. Typical thrust measurements are plotted in Fig. 17 (Jones et al. 2005). Another important advance was the excitation system which consists of two swing arms which are driven by a crankshaft and scotch yoke combination. This mechanism oscillates the two airfoils in plunge. Yet, as already mentioned, it is desirable to have a joint pitch/plunge oscillation with a 90° phasing between the two oscillations. This requirement was met by mounting the airfoils elastically at the ends of the swing arms, thus providing the airfoils with the desired pitch degree of freedom by properly adjusting the stiffness of the connection to the swing arms.

6 Experimental tests of the complete micro air vehicle

Having thus solved the thrust generation problem, it remained to size the stationary wing in order to obtain sufficient lift and provide it with reflex camber and sweep or dihedral for longitudinal and lateral stability. These considerations led to the wind tunnel model shown in Fig. 18. The pendulum arrangement used in the previous studies to measure thrust/drag was not suitable for measuring both lift and thrust, so a rotating arm test stand

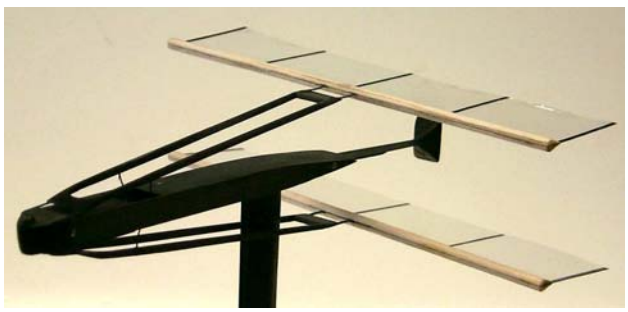

Fig. 15 MAV-sized flapping-wing propulsion model. The *small black square* behind the wings is a reflective surface for the laser range finder

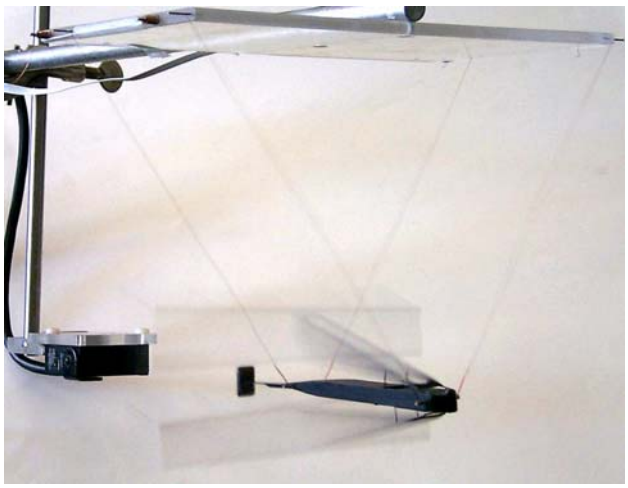

Fig. 16 Pendulum arrangement for wind-tunnel testing. The model is suspended on 0.08 mm diameter copper wires which also provide power and sensing for the stepping motor. The laser range finder is seen about 15 cm downstream

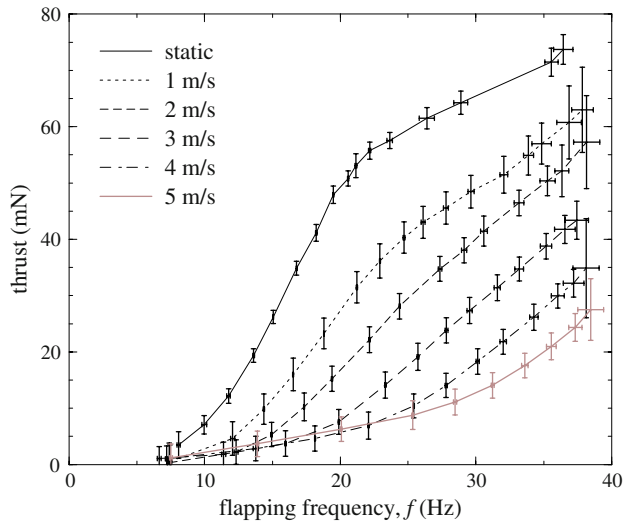

Fig. 17 Typical results from the 15 cm biplane test model. Reynolds numbers ranged from 0 to 12,000

(shown in Fig. 19) was devised. The model would propel itself around the central axis, and a hinge mount at the end of the rotating arm allowed the model to support its own weight with lift. Static thrust for this model was comparable to that shown in Fig. 17.

The results of this study provided sufficient knowledge to size a complete vehicle (shown in Fig. 1) to carry the power and control components available at the time. Having a successful free flying configuration, we then built a wind-tunnel variation, shown in Fig. 20, and performed direct force measurements, flow-visualization and LDV experiments in a low-speed wind-tunnel. Flow visualization was accomplished with a smoke wire which was constructed from 0.25 mm diameter NiCr beaded wire,

Fig. 18 First complete MAV prototype with a fixed forward wing for lift. Span length = 15 cm

heated by passing a current through it, and using Rosco Fog Juice as the smoke agent. The model was mounted at a 15° angle of attack, at a flow speed of about 2 m/s, approximating the low-speed flight conditions. In Fig. 21 we show the case when the flapping wings are at rest (left figure) or flapping at 30 Hz (right figure). The model is viewed from the left rear corner forward, providing a good view of the flow over the upper surface of the left wing. In the left figure it is clearly seen that the flow separated at the leading edge, exposing the wing to full stall. The powerful entrainment effect in suppressing stall is clearly seen in the right figure. It is also very fast acting. It took only about a tenth of a second (4 flapping strokes) to reattach the flow after activation of the flapping wings. Details of the flow visualization study are documented in Papadopoulos (2003).

Unsteady LDV measurements were made with a TSI two-channel system with a single probe and a Rosco fog generator for flow seeding. A rotary motion resolver (RMR) was used to resolve the oscillatory flow generated by the flapping wings. The measurement details are documented in Bradshaw (2003). In Fig. 22 we show the time-averaged velocity profile just in front of the flapping wings for three cases. In the first case, the main wing is removed, and the wings are flapped at 32 Hz. In the second case, the main wing is included, but the wings are not flapped. In the third case, the main wing is included and the wings are flapped at 32 Hz. In all three cases the free-stream speed is 2.75 m/s, and the model is set at a 15° angle of attack. Due to the dihedral of the main wing, a large area above the symmetry plane was inaccessible to the laser, thus yielding detailed results only for the lower flapping wing. Without wing flapping, a velocity defect is seen, whereas wing flapping generates a significant entrainment effect (with or without the presence of the main wing).

Fig. 19 Rotating-arm test stand for the MAV to measure lift and drag

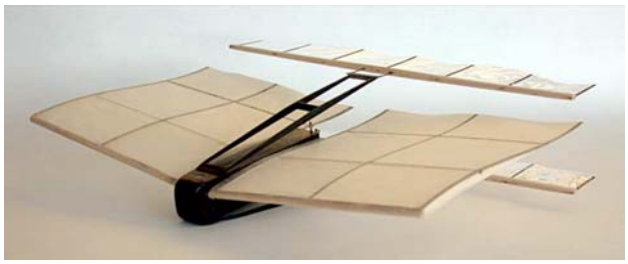

Fig. 20 Wind-tunnel variant of the first flying model with continuous-duty motor and optical encoder

7 Summary and outlook

It was the objective of this paper to describe the experiments which we conducted to develop the flapping-wing micro air vehicle shown in Fig. 1. The decision to use flapping wings rather than conventional propellers was "bio-inspired" by our belief that flapping wings might have propulsive and aerodynamic characteristics superior to conventional vehicles at the Reynolds numbers required for micro air vehicle flight. However, we resisted the temptation to "mimic" bird flight to the maximum possible extent (i.e. develop a biomimetic vehicle). Instead, we based our initial design concept on the information available in the early 1990s which was largely confined to inviscid two-dimensional flow analyses of oscillating airfoils. This state-of-the-art led us to the recognition that experiments were needed to examine the validity of ideal-flow analyses. It also led us to the conclusion that it might be advantageous to base the design on high-aspect ratio wings which are flapping with constant spanwise amplitude. This choice made it possible to limit the experiments (and additional viscous flow analyses) to two-dimensional flow studies while, at the same time, avoiding the thrust (and lift) losses incurred by birds whose flapping amplitude approaches zero toward the wing roots. Therefore, our vehicle is a biomorphic vehicle whose design is based on selecting only certain features found in nature. In fact, we deliberately adopted conventional aircraft design methods by continuing to use separate propulsion and lifting systems. We argued that it would be quite difficult to use flapping-wings for both thrust and lift

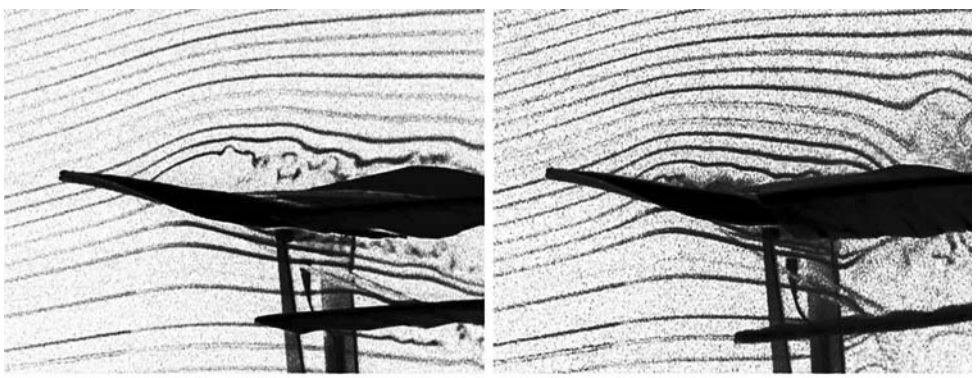

Fig. 21 View of the model in Fig. 21 from the left rear, with the flow coming from left to right. In the *left image* the aft wings are stationary, and the flow over the main wing is separated. In the *right image*, the trailing wings have started flapping and have just completed four flapping strokes, and the flow over the main wing is already reattached. For this extreme case, $\alpha = 15°$, $f = 30$ Hz and $V_\infty = 2$ m/s resulting in Reynolds numbers of 20,000 for the main wing, and 5,500 for the flapping wings

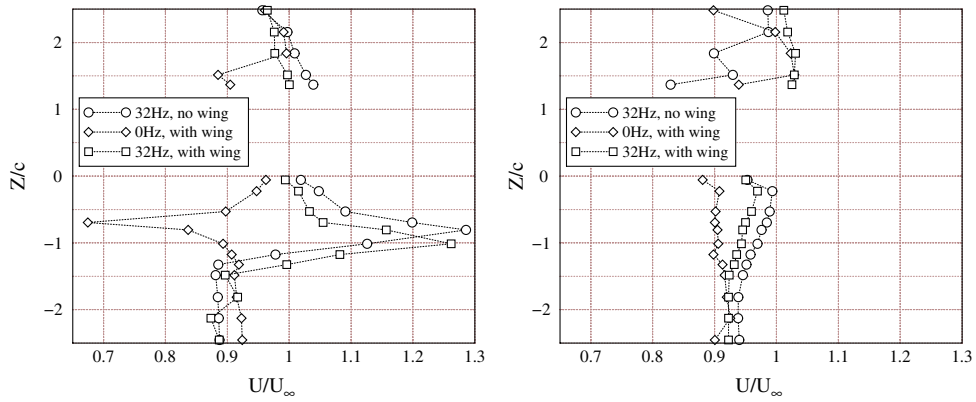

Fig. 22 Time-averaged LDV results illustrating the flow entrainment at the leading edges of the flapping wings. In the *left image*, the velocity is measured essentially at the leading edges of the flapping wings. In the *right image*, the velocity is measured a chordlength upstream of the leading edges. *Z*/*c* is the vertical distance from the centerline. Note that the region from 0 to 1.5 is masked by the main wing. Flow conditions were $V_\infty = 2.75$ m/s and $\alpha = 15°$

generation. Therefore, we concentrated on understanding the physics of thrust generation by high-aspect ratio flapping-wings and resorted to the use of fixed wings for lift generation.

The experiments described in this paper therefore focused at first on the determination of the effect of amplitude and frequency on the flow physics and on the thrust generated by two-dimensional plunging airfoils. The insight obtained from these studies then led to the exploration of the effectiveness of flapping airfoils as flow control devices. These studies revealed the advantages to be obtained from using two airfoils (flapping in counterphase) in close vicinity (but downstream) from a fixed wing.

Although the information obtained in the course of our experimental and computational studies was sufficient for the development of a successful flapping-wing micro air vehicle (Fig. 1). A number of aerodynamic aspects require further exploration. Little aerodynamic design information is available on three-dimensional flow effects for flapping-wings in forward flight. Flapping-wing micro air vehicles that can take-off and land vertically, hover, maneuver and fly forward are likely to require a detailed understanding of the complex aerodynamics of humming birds or insects. Hence, as reviewed in Platzer et al.(2008), many challenging unsteady aerodynamic flows remain to be studied experimentally and computationally in the field of low Reynolds number aerodynamics with applications to the development of micro air vehicles.

Acknowledgments We are grateful for the support received from Spiro Lekoudis of the Office of Naval Research, with project monitors Peter Majumdar and Edwin Rood, and from Richard Foch, head of the Vehicle Research Section of the Naval Research Laboratory, with project monitors Kevin Ailinger, Jill Dahlburg and James Kellogg. We would also like to acknowledge the contributions of Jiannwoei Yue, Claus Dohring, Joseph Lai, John Young, Jason Papadopoulos and Chris Bradshaw.

References

Betz A (1912) Ein beitrag zur erklaerung des segelfluges. Zeitschrift fuer Flugtechnik und Motorluftschiffahrt 3:269–270

Betz A (1966) Introduction to the theory of flow machines. Pergamon, New York

Birnbaum W (1924) Das ebene problem des schlagenden fluegels. Zeitschrift fuer Angewandte Mathematik und Mechanik 4(4):277–290

Bradshaw CJ (2003) An experimental investigation of flapping wing aerodynamics in micro air vehicles. Master's thesis, Department of Aeronautics and Astronautics, Naval Postgraduate School, Monterey

Bratt JB (1950) Flow patterns in the wake of an oscillating airfoil. Technical Report R & M 2773, Aeronautical Research Council

Dalton S (1999) The miracle of flight. Firefly Books, Westport

Dohring CM (1998) Der Schub des schlagenden Fluegels und seine Anwendung zur Grenzschichtbeeinflussung. PhD thesis, German Armed Forces University, Munich

Garrick IE (1936) Propulsion of a flapping and oscillating airfoil. Technical Report 567, NACA

Heathcote S, Gursul I (2004) Jet switching phenomenon for a plunging airfoil. AIAA-2004-2150

Jones KD, Dohring CM, Platzer MF (1998) Experimental and computational investigation of the Knoller-Betz effect. AIAA J 36(7):1240–1246

Jones KD, Lund TC, Platzer MF (2001) Fixed and flapping wing aerodynamics for micro air vehicle applications, vol 195, Progress in Astronautics and Aeronautics, Chap 16, Experimental and computational investigation of flapping wing propulsion for micro air vehicles, pP 307–339. AIAA

Jones KD, Bradshaw CJ, Papadopoulos J, Platzer MF (2005) Bio-inspired design of flapping-wing micro air vehicles. Aeronaut J Roy Aeronaut Soc 109(1098):385–392

Katzmayr R (1922) Effect of periodic changes of angle of attack on behavior of airfoils. Technical Report TM 147, NACA

Knoller R (1909) Die gesetze des luftwiderstandes. Flug- und Motortechnik 3(21):1–7

Lai JCS, Platzer MF (1999) Jet characteristics of a plunging airfoil. AIAA J 37(12):1529–1537

Lai JCS, Yue J, Platzer MF (2002) Control of backward-facing step flow using a flapping foil. Exp Fluids 32:44–54

Lilienthal O (1992) Der Vogelflug als Grundlage der Fliegekunst, 3rd edn. Harenberg Kommunikation, Dortmund

Papadopoulos JP (2003) An experimental investigation of the geometric characteristics of flapping-wing propulsion for a micro air vehicle. Master's thesis, Department of Aeronautics and Astronautics, Naval Postgraduate School, Monterey

Platzer MF, Neace KS, Pang KC (1993) Aerodynamic analysis of flapping wing propulsion. AIAA-93-0484

Platzer MF, Jones KD, Young J, Lai JCS (2008) Flapping-wing aerodynamics: progress and challenges. AIAA J 46(9):2136–2149

Smith LH (1947) Wake ingestion propulsion benefit. J Propuls Power 9(1):74–82

Smith AMO, Roberts HE (1947) The jet airplane utilizing boundary layer air for propulsion. J Aeronaut Sci

Teng NH (1987) The development of a computer code for the numerical solution of unsteady inviscid and incompressible flow over an airfoil. Master's thesis, Department of Aeronautics and Astronautics, Naval Postgraduate School

Theodorsen T (1935) General theory of aerodynamic instability and the mechanism of flutter. Technical Report 496, NACA

von Kármán T, Burgers JM (1934) General aerodynamic theory-perfect fluids, aerodynamic theory, vol II. Julius Springer, Berlin